Understanding the affinity of bis-exTTF macrocyclic receptors towards fullerene recognition

J. Calbo, A. de Juan, J. Aragó, J. Villalva, N. Martín, E. M. Pérez and E. Ortí

Understanding the affinity of bis-exTTF macrocyclic receptors towards fullerene recognition

Joaquín Calbo,*[a] Alberto de Juan,[b] Juan Aragó,[c] Julia Villalva,[b] Nazario Martín,[d,e] Emilio M. Pérez,*[e] Enrique Ortí*[c]

A new series of fullerene receptors based on exTTF macrocycles with alkyl ether chains of increasing length is reported. The novel macrocyclic receptors are able to favourably interact with fullerene C_{60} through a synergistic combination of π–π, CH···π and n···π noncovalent interactions. We identify that the highest affinity towards C_{60} recognition is achieved for the host with the tightest fit; that is, the smallest receptor with a cavity large enough to host the buckyball inside (log K_a = 5.2 in chlorobenzene at 298 K). However, besides this expected observation, theoretical calculations evidence that the most stable self-assembling configuration corresponds for all the receptors to an outside-ring binding mode, in which the C_{60} guest is out of the cavity of the receptor. The higher stability of this configuration results from the smaller deformation energy it implies for the receptor, and allows to explain the experimental trends in the association constants.

Introduction

The synthetic design of supramolecular receptors of fullerenes and buckybowls is a very active field of research, which has found application in the selective extraction of fullerenes from complex mixtures and in the construction of multifunctional supramolecular self-assemblies.[1–9] Moreover, the electron-acceptor ability of fullerenes and fullerene fragments (buckybowls) has been elegantly combined with electron-rich receptors to produce electroactive nanostructures that can be used for light harvesting and artificial photosynthesis.[10–15] Just seven years after the discovery of fullerenes, the first design of fullerene receptors was accomplished by Ringsdorf *et al.* in 1992.[16] Thenceforth, a maddening race for achieving higher affinities towards fullerene recognition has led to the discovery of receptors based on calix[*n*]arenes, corannulenes, π-extended tetrathiafulvalenes (TTFs), and porphyrins, to name a few of them.[2,3,17–23] Among them, Ir(III) metalloporphyrin derivatives reported by Yanagisawa *et al.* present one of the largest complex stabilities, with a log K_a = 8.1 for C_{60} in 1,2-dichlorobenzene at room temperature,[24] only surpassed by a molecular peapod reported by Isobe *et al.*,[25] which holds the record with a log K_a = 9.6 under the same experimental conditions.

The TTF-based, electron-rich 9,10-bis(1,3-dithiol-2-ylidene)-9,10-dihydroanthracene moiety (exTTF) has gained increasing attention in the last years to build efficient receptors for C_{60} and other carbon nanostructures such as nanotubes[26–28] and graphene.[3,29–31] Moreover, exTTF-based receptors have demonstrated to promote interesting electron-transfer phenomena with these carbon-based nanomaterials upon light irradiation,[10,32,33] and they have recently been employed in the development of mechanically-interlocked nanotube derivatives.[34,35]

Thanks to its particular butterfly or saddle-like shape, exTTF is able to favourably interact with buckyballs through a concave–convex structural complementarity that maximizes π–π noncovalent interactions.[30] In 2006, some of us reported the first exTTF-based fullerene receptor based on a tweezer-like design.[36] Importantly, substitution of the dithiole moieties by other functional groups allowed discerning the effect of size, shape and electronic character of the recognizing motifs, demonstrating that π–π forces are the main driving force for the self-assembly.[37] More recently, decoration of a pincer-like exTTF receptor with an alkyl linker led to the highest complex affinity for this kind of derivatives towards C_{60} recognition, with a log K_a = 6.5 in chlorobenzene at 298 K.[38] The exTTF-based macrocycle reported by Isla *et al.* was demonstrated to provide high affinity towards fullerene owing to a combination of π–π and CH···π noncovalent interactions. Moreover, small variations in the structure of the receptor led to significant changes into the complexation strength with C_{60}, and even in the stoichiometry of the host–guest complexes.[39] However, no clear structure–property relationship

[a] *Instituto de Ciencia Molecular, Universidad de Valencia, 46890 Paterna (Valencia), Spain. Current address: Department of Materials, Imperial College London, London SW7 2AZ, United Kingdom.*
[b] *Chemistry, University of Southampton, Highfield Southampton, SO17 1BJ, United Kingdom.*
[c] *Instituto de Ciencia Molecular, Universidad de Valencia, 46890 Paterna (Valencia), Spain.*
[d] *Departamento de Química Orgánica I, Facultad de Química, Universidad Complutense de Madrid, Avda. Complutense s/n, 28040 Madrid, Spain.*
[e] *IMDEA-Nanociencia, c/Faraday 9, Campus Cantoblanco, 28049 Madrid, Spain.*

could be found to explain the trends in log K_a upon variation of the length of the alkyl linker in the macrocycle.

Herein, we report a new series of exTTF-based macrocyclic receptors of C_{60} fullerene, where two electron-donor exTTF moieties are connected through an alkyl ether linker with terminal alkenes to achieve macrocyclization (Scheme 1). The combination of π–π interactions originated in the exTTF region together with the CH···π and lone-pair *n*···π forces promoted by the ether chains result in high complexation stability towards C_{60} in all receptors. Theoretical calculations allowed dissecting the energetic contributions to explain the fullerene affinity trends obtained experimentally, and provide guidelines for future design of improved fullerene receptors.

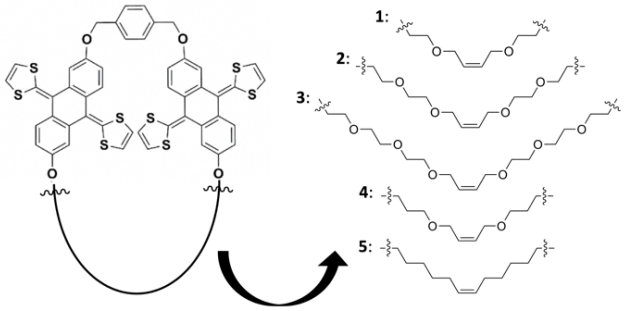

Scheme 1 Chemical structure of the new exTTF-based macrocycles **1**–**4** with alkyl ether chains, and the previously reported receptor **5** with alkyl chains.[38]

Results and discussion

An initial exploration of different exTTF-based macrocycles containing alkyl ether chains of different lengths was carried out through a nanotube-expansion modelling protocol.[35] The exTTF receptors (or hosts) **1**–**4** were designed in an open conformation to bear a *zig–zag* single-walled nanotube SWNT (*n*,0) with *n* = 8) inside, and the binding energy was calculated at the semiempirical PM7 level upon increasing the nanotube diameter (see the ESI† for details). The efficient receptor **5** with alkyl chains reported by some of us is included for comparison purposes.[38] The size of the macrocycle was calculated by using the most expanded geometry of the receptor for which the binding energy of the exTTF·SWNT complex is still stable (Fig. S2†). Table 1 summarizes the calculated effective diameter (d_{eff}) of the exTTF-based receptors compared with that for the fullerene C_{60} guest.

Table 1 Effective diameter (d_{eff}) for the ring cavity inside the macrocyclic exTTF host ($d_{h,eff}$) and for the fullerene guest ball ($d_{g,eff}$).[a]

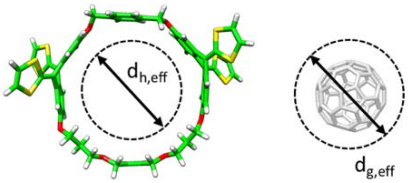

System	d_{eff} (Å)
1	9.8
2	11.6
3	13.9
4	10.5
5	10.8
C_{60}	10.5

[a] Effective diameters are calculated in a simplistic manner by removing (in the host) or adding (in the buckyball) twice the van der Waals radius of a carbon atom (2 × 1.70 Å).

Theoretical calculations indicate that the smallest receptor **1**, with a d_{eff} = 9.8 Å is unable to host C_{60} (d_{eff} = 10.5 Å) inside due to its short ethylene glycol chains and, therefore, a very low C_{60} affinity is expected for this macrocycle. Otherwise, increasing the alkyl ether chain in receptors **2** and **3** leads to macrocycles with ring cavities large enough to accommodate the buckyball (d_{eff} = 11.6 and 13.9 Å, respectively). Receptor **4**, containing 1,3-propylene glycol groups and showing a d_{eff} = 10.5 Å, perfectly fits the fullerene size (Table 1), and might provide an optimal receptor for C_{60} due to its complementarity. Note that, in comparison with the ether-based receptor **4**, the efficient receptor **5** containing alkyl chains provides a slightly larger d_{eff} of 10.8 Å as the C–C distance in the alkyl chain (1.52 Å) is larger than the ether C–O distance (1.43 Å).

Encouraged by the theoretical outcomes, receptors **1**–**4** were then synthesized following the procedure described in the ESI. Briefly, halogenated glycolic derivatives were obtained through mono-alkylation reaction of the corresponding commercial glycol with allyl bromide, followed by nucleophilic substitution of alcohol by halogen atom. Then, anthraflavic acid was reacted with the corresponding alkenyl glycols, yielding the mono-alkyl derivate of anthraflavic acid. Dialkylation of α,α-dibromo-*p*-xylene with these anthraflavic acid derivatives, followed by Horner–Wadsworth–Emmons olefination, afforded the *U*-shaped macrocycle precursors. The final compounds **1**–**4** were obtained through ring closing metathesis (RCM) reaction of the precursor in presence of first-generation Grubbs catalyst. Macrocyclic receptors were isolated as an inseparable mixture of *Z* and *E* isomers, which were used as such.

To measure the binding constants of the exTTF-based macrocycle·C_{60} complexes, we performed a set of UV-vis titrations in chlorobenzene (PhCl) at room temperature. Every binding constant is estimated as an average of three independent experiments, and the error is reported as the standard deviation. In a typical titration, we work at constant concentration of host to avoid dilution effects (see the ESI†). To ensure saturation, we added portions of the C_{60} solution to the host solution, and the titration was stopped after three equivalents of fullerene. After each addition, UV-vis spectra were

recorded, and the spectroscopic data obtained was analyzed with Reactlab Equilibria™ analysis software to estimate the association constant.

Through qualitative analysis of the UV-vis data, we can observe that the titration experiments of the four host–guest systems show the same behavior (Fig. 1). Specifically, the main absorption band corresponding to the exTTF subunits at λ_{max} = 428 nm decreases after addition of aliquots of [60]fullerene. When the concentration of fullerene increases, besides the typical absorption features of free C_{60}, a charge-transfer band appears at λ_{max} = 480–485 nm with the formation of an isosbestic point at λ = 442 nm for all the titrations. These changes in the absorption spectra unambiguously show that the complexation between the host and guest takes place. All the UV-vis spectra data were best fit by using a 1:1 supramolecular equilibrium model.[40] From these analyses, we extract binding constants. Macrocycle **2** presents a log K_a = 3.7 ± 0.2, that is the lowest value obtained for this family of molecular receptors. Compounds **1** and **3** show very similar binding constants, log K_a = 4.6 ± 0.4 and 4.1 ± 0.7, respectively. The highest affinity towards C_{60} is found for the receptor with the smallest ring capable of bearing C_{60} inside (macrocycle **4**), that presents a log K_a = 5.2 ± 0.7. Surprisingly, receptor **1**, which according to calculations is not able to accommodate C_{60} inside its cavity, still shows high affinity, with an association constant comparable to those of **2** and **3** (Table 2).

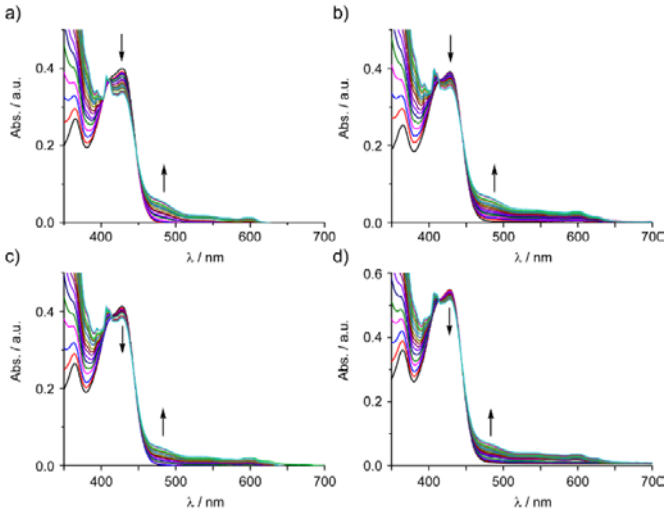

Fig. 1 Spectral changes in UV-vis titration experiments in PhCl at room temperature of (a) **1**·C_{60}, (b) **2**·C_{60}, (c) **3**·C_{60} and (d) **4**·C_{60}.

Table 2 Binding constants, presented as log K_a, and the corresponding binding free energy ($\Delta G_{bind,exp}$, in kcal/mol) for the different molecular receptors towards C_{60}.[a]

Complex	log K_a	$\Delta G_{bind,exp}$
1·C_{60}	4.6 ± 0.4	–6.3
2·C_{60}	3.7 ± 0.2	–5.0
3·C_{60}	4.1 ± 0.7	–5.6
4·C_{60}	5.2 ± 0.7	–7.1
5·C_{60}	6.5 ± 0.5 [b]	–8.9

[a] Every experiment was repeated 3 times. Standard deviation is indicated as error for the log K_a. [b] Value extracted from Ref. [38].

To better understand the receptor-fullerene self-assembling process, theoretical calculations were performed at the molecular mechanics/molecular dynamics (MM/MD) level in gas phase. The complexation potential mean force (PMF) profiles (Fig. 2) were calculated for **1**–**5**·C_{60} using the general MM3 force-field and the weighted histogram analysis method (WHAM). The host and guest centroids were used to define a constraint distance (host–guest distance in Fig. 2), and to sample the region comprising the fullerene centred inside the macrocycle cavity (structure 1 in Fig. 2) and the fully dissociated complex (structure 4, Fig. 2). The WHAM method was employed with 40 windows and 1000 integration points at room temperature (see the ESI† for full computational details)

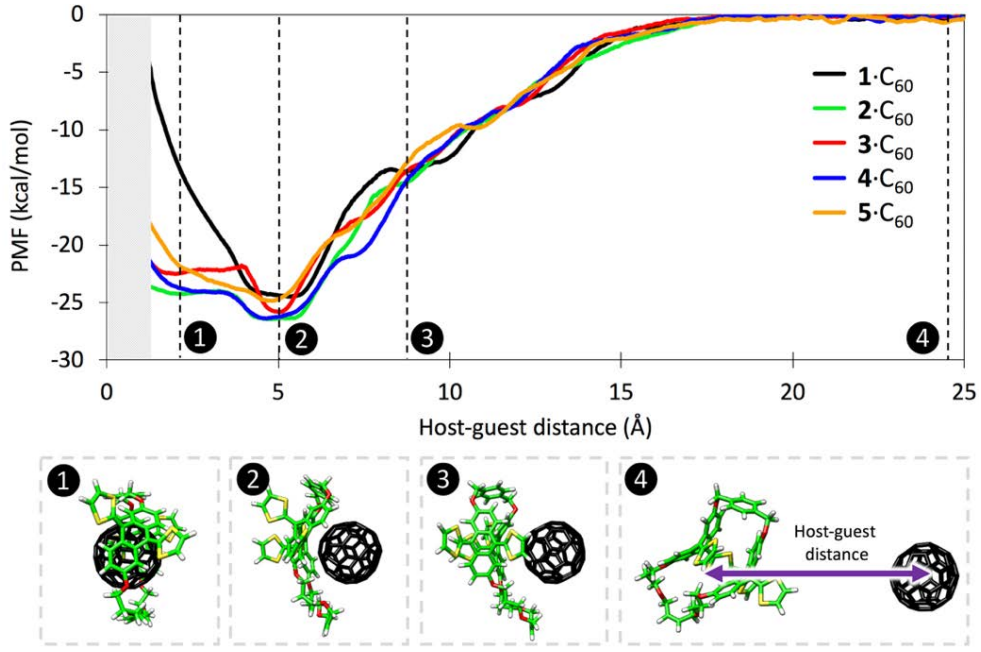

Fig. 2 Potential mean force (PMF) profile for the receptor-fullerene self-assembling process. Representative structures at different points of the PMF profile are displayed for **4**·C_{60} (bottom). The region < 1 Å (in grey) is not physically meaningful due to the definition of the host–guest distance between centroids and is therefore omitted.

The theoretical PMF profile gives valuable information on the events occurring during the receptor·fullerene self-assembly. The main differences between receptors are found at short host–guest distances in the PMF profile (< 5 Å in Fig. 2). For **1**·C_{60}, the binding energy decreases and the PMF scales up upon shortening the host–guest distance from 5 Å. This is in line with the initial geometry analysis of the cavity size (see above and Table 1), suggesting that receptor **1** is unable to host the fullerene ball inside its ring. Conversely, increasing the chain length in hosts **2**–**5** leads to a plateau minimum in the ca. 2.5 Å region with a PMF of ca. –22 kcal/mol. In this region, the fullerene is placed inside the macrocycle cavity ("inside-ring" adsorption mode; structure 1 in Fig. 2).

Unexpectedly, a slightly deeper well of around –25 kcal/mol is predicted for all receptors at longer host–guest distances (Fig. 2), indicating a somewhat more favourable interaction between **1**–**5** and C_{60}. The minimum of the well is positioned at a host–guest distance of ca. 5 Å, suggesting that the fullerene is not placed in the centre of the receptor cavity. A careful inspection of the geometry indicates that the minimum-energy structures at 5 Å correspond to a self-assembling mode in which the fullerene is outside the ring cavity of the macrocycle and the receptor embraces the buckyball in a concave–convex fashion ("outside-ring" adsorption mode; structure 2 in Fig. 2).

The binding free energy of the self-assembling process ($\Delta G_{\text{bind,theor}}$) between the exTTF-based macrocycles **1**–**5** and fullerene C_{60} in chlorobenzene was theoretically quantified by taking into account the enthalpic, entropic and solvent effects through first-principles density functional theory (DFT) calculations performed at the B97D3/6-31G** level (see the ESI† for computational details). Note that the binding energy (ΔE_{bind}) can be decomposed according to:

$$\Delta E_{\text{bind}} = \Delta E_{\text{int}} + E_{\text{def}}$$

where ΔE_{int} and E_{def} are the interaction and deformation energy, respectively. ΔE_{int} is the stabilizing energy between the two monomers when combined in the complex, and is defined as:

$$\Delta E_{\text{int}} = E_{\text{AB}}^{\text{AB}} - E_{\text{A}}^{\text{AB}} - E_{\text{B}}^{\text{AB}}$$

where E_{X}^{Y} denotes the energy of system X at the geometry of system Y, being the system either one of the two monomers A and B or the

complex AB. Otherwise, E_{def} is the energy penalty required for the monomers to move from their relaxed geometry to the geometry in the dimer, and is calculated according to:

$$E_{\mathrm{def}} = \left(E_{\mathrm{A}}^{\mathrm{AB}} - E_{\mathrm{A}}^{\mathrm{A}}\right) + \left(E_{\mathrm{B}}^{\mathrm{AB}} - E_{\mathrm{B}}^{\mathrm{B}}\right)$$

Due to the large conformational space in our macrocyclic receptors, and the rigidity of the fullerene moiety, the deformation energy can be assigned to the macrocycle only (see ESI†, Table S3) and split into two contributions (Fig. 3): the energy loss due to the rupture of the intramolecular noncovalent interactions in the relaxed entangled receptor ($E_{def,intra}$), and the deformation coming from the macrocycle disposition upon complexation ($E_{def,complex}$). Thus,

$$E_{\mathrm{def}} \approx E_{\mathrm{def,host}} = E_{\mathrm{def,intra}} + E_{\mathrm{def,complex}}$$

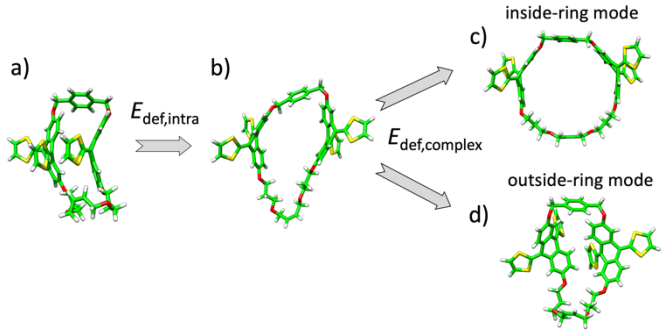

Fig. 3 Schematic representation of the two contributions to the total deformation energy in the exTTF-based macrocyclic receptors: the deformation energy due to the rupture of the intramolecular noncovalent interactions ($E_{def,intra}$), and the deformation to accommodate the fullerene guest ($E_{def,complex}$). The minimum-energy structures for receptor **4** in its most stable conformation (a), in an open-ring conformation (b), and in the geometry adopted in the inside-ring (c) and outside-ring (d) modes of the host-guest complex are displayed.

Table 3 Thermodynamic parameters (in kcal/mol) calculated for the inside-ring and outside-ring adsorption modes in the **1**–**5**·C_{60} complexes at the B97D3/6-31G** level of theory.

Complex	ΔE_{int}	$E_{def,complex}$	$E_{def,host}$	ΔE_{bind}	$\Delta G_{bind,theor}$
inside-ring mode					
1·C_{60}[a]	-	-	-	-	-
2·C_{60}	–59.9	5.3	36.9	–22.4	2.8
3·C_{60}	–62.4	–1.3	42.3	–19.7	5.2
4·C_{60}	–58.1	2.6	33.6	–23.9	1.2
5·C_{60}	–58.9	7.2	33.5	–24.8	0.0
outside-ring mode					
1·C_{60}	–48.9	–14.0	14.5	–34.3	–3.2
2·C_{60}	–52.3	–14.4	17.2	–34.7	–4.3
3·C_{60}	–59.8	–21.0	22.7	–37.2	–4.8
4·C_{60}	–50.5	–16.9	14.1	–36.5	–6.1
5·C_{60}	–49.9	–12.2	14.0	–32.5	–6.3

[a] An outside-ring mode with an opened ring macrocycle resembling the inside-ring mode is found for **1**·C_{60}. This adsorption mode offers the following thermodynamic parameters: ΔE_{int} = –53.52 kcal/mol, $E_{def,complex}$ = 6.18 kcal/mol, $E_{def,host}$ = 34.6 kcal/mol, ΔE_{bind} = –18.82 kcal/mol and $\Delta G_{bind,theor}$ = 6.31 kcal/mol.

The interaction energy (ΔE_{int}) calculated at the B97D3/6-31G** level for the host–guest complexes increases with the size of the macrocyclic receptor: from –58.1 kcal/mol in **4**·C_{60} to –62.4 kcal/mol in **3**·C_{60} for the inside-ring mode, and from –48.9 kcal/mol in **1**·C_{60} to –59.8 kcal/mol in **3**·C_{60} for the outside-ring mode. Absolute values of ΔE_{int} are computed larger for the inside-ring mode, suggesting a more favourable interaction with C_{60} in this adsorption configuration. However, calculation of the ΔE_{bind} upon inclusion of the deformation energy leads to a different scenario, where the outside-ring structures are found more than 10 kcal/mol more stable than the corresponding inside-ring configurations (Table 3). These trends can easily be correlated with the complexation deformation energy ($E_{def,complex}$) due to the accommodation of the macrocyclic receptor to bind C_{60}. In the case of the inside-ring mode, the macrocycle adopts an unfavourable strained configuration in the complex (Fig. 3c), leading to a positive value of $E_{def,complex}$; only the largest macrocycle **3** offers a small negative value for this deformation term (Table 3). In contrast, $E_{def,complex}$ is found largely negative for the outside-ring configuration (from –12.2 in **5**·C_{60} to –21.0 in **3**·C_{60}), suggesting that the macrocycle is interacting with itself favourably by means of intramolecular noncovalent forces in the supramolecular complex geometry (see Fig. 3d). Note that $E_{def,intra}$ is calculated positive for both inside- and outside-ring modes with values in the range of [26.3,43.6] kcal/mol (see Table S3 in the ESI†). These results are in line with a recent study on triazole-based receptors for C_{60} reported by some of us, where outside-ring self-assembling configurations similar to those predicted in the present work were found energetically relevant.[41]

The inclusion of the enthalpy, entropy and solvation corrections to ΔE_{bind} allowed us to estimate the binding free energy, to be compared with the experimental values summarized in Table 2 (see the ESI† for a detailed explanation of the calculation of $\Delta G_{bind,theor}$ and Table S4 for the tabulated contributing terms). Theoretical calculations predict positive $\Delta G_{bind,theor}$ values for all the inside-ring adsorption complexes as a result of the large deformation energy of the macrocyclic host (Table 3), and point to their energetically unfavoured formation. In contrast, $\Delta G_{bind,theor}$ values in the range of [–6.3,–3.2] kcal/mol are calculated for the outside-ring adsorption modes, which nicely agree with the experimental binding affinities found for the studied receptor·C_{60} complexes (range of [–8.9,–5.0] kcal/mol, Table 2). The largest macrocycle **3**, which shows the highest binding energy towards fullerene, is predicted to provide a modest $\Delta G_{bind,theor}$ of –4.8 kcal/mol due to the counterbalance of large and positive entropic and solvation terms (Table S4). In contrast, macrocycle **4** presents the best trade-off between binding energy, entropy and solvation effects due to its relatively small alkyl ether chain (Table S4). As a result, **4** shows the highest C_{60} affinity among the exTTF macrocycles based on alkyl ether chains ($\Delta G_{bind,theor}$ = –6.1 kcal/mol), in good accord with the experimental evidences (Table 2).

We finally analysed the origin of the high affinity found in our novel exTTF macrocycles to bind fullerene C_{60}. Fig. 4a displays the minimum-energy structure calculated for **4**·C_{60} as a representative example (see Fig. S4 for the inside-ring mode of **4**·C_{60}). In the most stable outside-ring adsorption mode, the receptor embraces the buckyball guided by the concave–convex complementarity between the butterfly shape of the exTTF moieties and the external convex part of fullerene. This leads to a large surface of π–π noncovalent interactions in the range of 3.2–3.6 Å (Fig. 4a), which can be visualized by the noncovalent interaction index (NCI) surface (Fig. 4b).[42,43] Importantly, the long alkyl ether chains fully interact with the fullerene ball, leading to a large surface of both CH···π (2.7–3.0 Å) and *n*···π (3.4–3.8 Å) noncovalent interactions (Fig. 4). The incorporation of alkyl ether chains can therefore be viewed as an appealing strategy to design novel receptors with enhanced affinity towards fullerene buckyballs and other related derivatives.

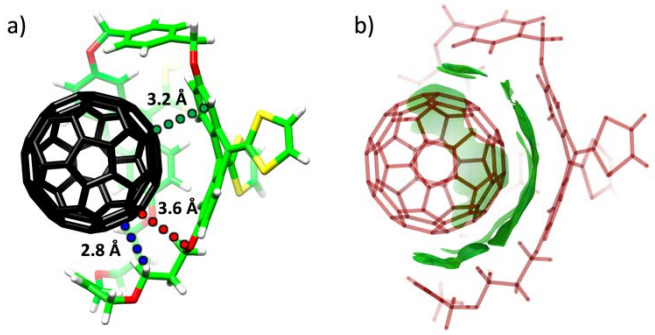

Fig. 4 Noncovalent interactions participating in the stabilization of the most stable outside-ring self-assembling mode of **4**·C_{60}: a) characteristic intermolecular contacts (π–π in green, *n*···π in red and CH···π in blue), and b) intermolecular NCI surface.

Conclusions

In summary, a new series of exTTF-based macrocyclic receptors bearing ethylene glycol chains has been synthesized, and their binding affinity towards fullerene C_{60} has been quantified experimentally and theoretically. The macrocycle possessing the minimum size to host C_{60} inside (i.e., the tightest fit) is demonstrated to provide the largest association constant. However, a smaller macrocycle that is not able to accommodate the buckyball inside also presents high affinity to bind C_{60}. We have identified two interacting configurations towards fullerene recognition that explain these data: inside-ring and outside-ring host–guest adsorption modes. The outside-ring mode is found to be the most stable self-assembling configuration, owing to its smaller deformation energy, and allows understanding the experimental trends found in the association constants upon inclusion of enthalpic, entropic and solvation effects. Theoretical calculations show that the novel macrocyclic receptors presented here favourably interact with the buckyball through a combination of π–π, CH···π and *n*···π noncovalent forces. The incorporation of alkyl ether chains is therefore demonstrated as an effective alternative to design efficient receptors for supramolecular fullerene recognition.

Conflicts of interest

There are no conflicts to declare.

Acknowledgements

Financial support by the European Research Council (307609), the MINECO of Spain (CTQ2015-71154-P, CTQ2017-86060-P, CTQ2017-83531-R, CTQ2016-81911-REDT, Centro de Excelencia Severo Ochoa SEV-2016-0686 and Unidad de Excelencia María de Maeztu MDM-2015-0538), Generalitat Valenciana (PROMETEO/2016/135 and SEJI/2018/035) and European Feder funds (CTQ2015-71154-P) is acknowledged. J.C. acknowledges the Generalitat Valenciana for an I+d+i postdoctoral fellowship (APOSTD/2017/081). J.A. is grateful to MINECO for a "Ramon-y-Cajal" fellowship (RyC-2017-23500).

Notes and references

1 E. M. Pérez and N. Martín, *Chem. Soc. Rev.*, 2008, **37**, 1512–1519.
2 N. Martin, J.-F. Nierengarten and Wiley InterScience (Online service), *Supramolecular chemistry of fullerenes and carbon nanotubes*, Wiley-VCH, 2012.
3 D. Canevet, E. M. Pérez and N. Martín, *Angew. Chemie Int. Ed.*, 2011, **50**, 9248–9259.
4 T. Nakanishi, *Chem. Commun.*, 2010, **46**, 3425–3436.
5 J. Calbo, J. Sancho-García, E. Ortí and J. Aragó, *Molecules*, 2018, **23**, 118.
6 L. Moreira, J. Calbo, B. M. Illescas, J. Aragó, I. Nierengarten, B. Delavaux-Nicot, E. Ortí, N. Martín and J. F. Nierengarten, *Angew. Chemie Int. Ed.*, 2015, **54**, 1255–1260.
7 L. Moreira, J. Calbo, J. Aragó, B. M. Illescas, I. Nierengarten, B. Delavaux-Nicot, E. Ortí, N. Martín and J. F. Nierengarten, *J. Am. Chem. Soc.*, 2016, **138**, 15359–15367.
8 M. Garrido, J. Calbo, L. Rodríguez-Pérez, J. Aragó, E. Ortí, M. Á. Herranz and N. Martín, *Chem. Commun.*, 2017, **53**, 12402–12405.
9 J. Calbo, J. Aragó, R. A. Boto, J. Sánchez-Marín, E. Ortí and J. Contreras-García, *J. Phys. Chem. A*, 2018, **122**, 1124–1137.
10 S. S. Gayathri, M. Wielopolski, E. M. Pérez, G. Fernández, L. Sánchez, R. Viruela, E. Ortí, D. M. Guldi and N. Martín, *Angew. Chemie Int. Ed.*, 2009, **48**, 815–819.
11 M. Gallego, J. Calbo, J. Aragó, R. M. Krick Calderon, F. H. Liquido, T. Iwamoto, A. K. Greene, E. A. Jackson, E. M. Pérez, E. Ortí, D. M. Guldi, L. T. Scott and N. Martín, *Angew. Chemie Int. Ed.*, 2014, **53**, 2170–2175.
12 M. Gallego, J. Calbo, R. M. K. Calderon, P. Pla, Y. C. Hsieh, E. M. Pérez, Y. T. Wu, E. Ortí, D. M. Guldi and N. Martín, *Chem. - A Eur. J.*, 2017, **23**, 3666–3673.
13 F. Wessendorf, B. Grimm, D. M. Guldi and A. Hirsch, *J. Am. Chem. Soc.*, 2010, **132**, 10786–10795.
14 B. Wang, S. Zheng, A. Saha, L. Bao, X. Lu and D. M. Guldi, *J.*

Am. Chem. Soc., 2017, **139**, 10578–10584.
15 B. Pelado, F. Abou-Chahine, J. Calbo, R. Caballero, P. de la Cruz, J. M. Junquera-Hernández, E. Ortí, N. V. Tkachenko and F. Langa, *Chem. - A Eur. J.*, 2015, **21**, 5814–5825.
16 J. Effing, U. Jonas, L. Jullien, T. Plesnivy, H. Ringsdorf, F. Diederich, C. Thilgen and D. Weinstein, *Angew. Chemie Int. Ed.*, 1992, **31**, 1599–1602.
17 E. M. Pérez, M. Sierra, L. Sánchez, M. R. Torres, R. Viruela, P. M. Viruela, E. Ortí and N. Martín, *Angew. Chemie Int. Ed.*, 2007, **46**, 1847–1851.
18 C. García-Simón, M. Costas and X. Ribas, *Chem. Soc. Rev.*, 2016, **45**, 40–62.
19 M. Takeda, S. Hiroto, H. Yokoi, S. Lee, D. Kim and H. Shinokubo, *J. Am. Chem. Soc.*, 2018, **140**, 6336–6342.
20 D. Canevet, E. M. Pérez and N. Martín, in *Organic Nanomaterials*, John Wiley & Sons, Inc., Hoboken, NJ, USA, 2013, pp. 147–162.
21 X.-S. Ke, T. Kim, J. T. Brewster, V. M. Lynch, D. Kim and J. L. Sessler, *J. Am. Chem. Soc.*, 2017, **139**, 4627–4630.
22 G. Gil-Ramírez, S. D. Karlen, A. Shundo, K. Porfyrakis, Y. Ito, G. A. D. Briggs, J. J. L. Morton and H. L. Anderson, *Org. Lett.*, 2010, **12**, 3544–3547.
23 G. Fernández, E. M. Pérez, L. Sánchez and N. Martín, *Angew. Chemie Int. Ed.*, 2008, **47**, 1094–1097.
24 M. Yanagisawa, K. Tashiro, A. Mikio Yamasaki and T. Aida, *J. Am. Chem. Soc.*, 2007, **129**, 11912–11913.
25 H. Isobe, S. Hitosugi, T. Yamasaki and R. Iizuka, *Chem. Sci.*, 2013, **4**, 1293–1297.
26 J. Calbo, A. López-Moreno, A. de Juan, J. Comer, E. Ortí and E. M. Pérez, *Chem. - A Eur. J.*, 2017, **23**, 12909–12916.
27 A. de Juan, A. López-Moreno, J. Calbo, E. Ortí and E. M. Pérez, *Chem. Sci.*, 2015, **6**, 7008–7014.
28 M. Á. Herranz, C. Ehli, S. Campidelli, M. Gutiérrez, G. L. Hug, K. Ohkubo, S. Fukuzumi, M. Prato, N. Martín and D. M. Guldi, *J. Am. Chem. Soc.*, 2007, **130**, 66–73.
29 L. Moreira, J. Calbo, R. M. Krick Calderon, J. Santos, B. M. Illescas, J. Aragó, J.-F. Nierengarten, D. M. Guldi, E. Ortí and N. Martín, *Chem. Sci.*, 2015, **6**, 4426–4432.
30 E. M. Pérez and N. Martín, *Chem. Soc. Rev.*, 2015, **44**, 6425–6433.
31 F. G. Brunetti, H. Isla, J. Aragó, E. Ortí, E. M. Pérez and N. Martín, *Chem. - A Eur. J.*, 2013, **19**, 9843–9848.
32 B. Grimm, J. Santos, B. M. Illescas, A. Muñoz, D. M. Guldi and N. Martín, *J. Am. Chem. Soc.*, 2010, **132**, 17387–17389.
33 E. Martínez-Periñán, A. de Juan, Y. Pouillon, C. Schierl, V. Strauss, N. Martín, Á. Rubio, D. M. Guldi, E. Lorenzo and E. M. Pérez, *Nanoscale*, 2016, **8**, 9254–9264.
34 E. M. Pérez, *Chem. - A Eur. J.*, 2017, **23**, 12681–12689.
35 A. de Juan, Y. Pouillon, L. Ruiz-González, A. Torres-Pardo, S. Casado, N. Martín, Á. Rubio and E. M. Pérez, *Angew. Chemie Int. Ed.*, 2014, **53**, 5394–5400.
36 E. M. Pérez, L. Sánchez, G. Fernández and N. Martín, 2006, **128**, 7172–7173.
37 E. M. Pérez, A. L. Capodilupo, G. Fernández, L. Sánchez, P. M. Viruela, R. Viruela, E. Ortí, M. Bietti and N. Martín, *Chem. Commun.*, 2008, **0**, 4567–4569.
38 H. Isla, M. Gallego, E. M. Pérez, R. Viruela, E. Ortí and N. Martín, *J. Am. Chem. Soc.*, 2010, **132**, 1772–1773.
39 D. Canevet, M. Gallego, H. Isla, A. de Juan, E. M. Pérez and N. Martín, *J. Am. Chem. Soc.*, 2011, **133**, 3184–3190.
40 D. Brynn Hibbert and P. Thordarson, *Chem. Commun.*, 2016, **52**, 12792–12805.
41 J. Mateos-Gil, J. Calbo, L. Rodríguez-Pérez, M. Ángeles Herranz, E. Ortí and N. Martín, *ChemPlusChem*, 2019, DOI: 10.1002/cplu.201900078.
42 E. R. Johnson, S. Keinan, P. Mori-Sánchez, J. Contreras-García, A. J. Cohen and W. Yang, *J. Am. Chem. Soc.*, 2010, **132**, 6498–6506.
43 J. Contreras-García, E. R. Johnson, S. Keinan, R. Chaudret, J.-P. Piquemal, D. N. Beratan and W. Yang, *J. Chem. Theory Comput.*, 2011, **7**, 625–632.